AD-A073 539 SCIENCE APPLICATIONS INC MCLEAN VA OCEAN SCIENCE DIV F/G 4/2
THE EFFECT OF INACCURACIES IN METEOROLOGICAL PARAMETERS ON ONE---ETC(U)
JUL 79 R M CLANCY N00014-78-C-0287
UNCLASSIFIED SAI-79-880-WA NL

1 OF 1
AD A073539

END
DATE FILMED
10-79
DDC

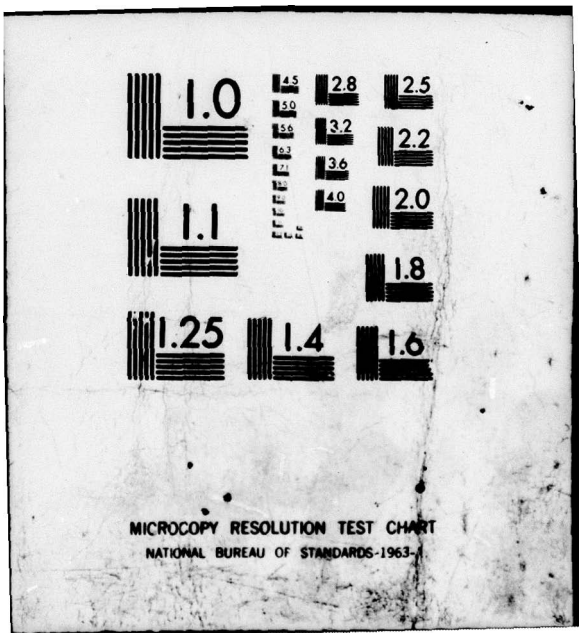
1.0
1.1
1.25
1.4
1.6
1.8
2.0
2.2
2.5
2.8
3.2
3.6
4.0
4.5
5.0
5.6
6.3
7.1
MICROCOPY RESOLUTION TEST CHART
NATIONAL BUREAU OF STANDARDS-1963-A

THE EFFECT OF INACCURACIES IN METEOROLOGICAL PARAMETERS ON ONE-DIMENSIONAL FORECASTS OF UPPER THERMAL STRUCTURE

SAI
ATLANTA • ANN ARBOR • BOSTON • CHICAGO • CLEVELAND • DENVER • HUNTSVILLE • LA JOLLA
LITTLE ROCK • LOS ANGELES • SAN FRANCISCO • SANTA BARBARA • TUCSON • WASHINGTON

THE EFFECT OF INACCURACIES IN METEOROLOGICAL PARAMETERS ON ONE-DIMENSIONAL FORECASTS OF UPPER OCEAN THERMAL STRUCTURE

SAI-79-880-WA

July 1979

Prepared by:

R. Michael Clancy*
Ocean Science Division

* Now at NORDA, Code 322
NSTL Station, MS 39529

SCIENCE APPLICATIONS, INC.
8400 Westpark Dr.
McLean, Virginia 22101
(703) 821-4300

UNCLASSIFIED

SECURITY CLASSIFICATION OF THIS PAGE (When Data Entered)

REPORT DOCUMENTATION PAGE		READ INSTRUCTIONS BEFORE COMPLETING FORM
1. REPORT NUMBER: SAI-79-880-WA	2. GOVT ACCESSION NO.	3. RECIPIENT'S CATALOG NUMBER
4. TITLE (and Subtitle): THE EFFECT OF INACCURACIES IN METEOROLOGICAL PARAMETERS ON ONE-DIMENSIONAL FORECASTS OF UPPER OCEAN THERMAL STRUCTURE.		5. TYPE OF REPORT & PERIOD COVERED: Final Report, 2/78 - 8/79 (Feb 78-Aug 79)
		6. PERFORMING ORG. REPORT NUMBER
7. AUTHOR(s): R. Michael Clancy		8. CONTRACT OR GRANT NUMBER(s): N00014-78-C-0287
9. PERFORMING ORGANIZATION NAME AND ADDRESS: Science Applications Inc. 8400 Westpark Drive McLean, VA 22102		10. PROGRAM ELEMENT, PROJECT, TASK AREA & WORK UNIT NUMBERS: 63R
11. CONTROLLING OFFICE NAME AND ADDRESS: NORDA Code 322 NSTL Station Mississippi 39529		12. REPORT DATE: July 1979
		13. NUMBER OF PAGES: 60
14. MONITORING AGENCY NAME & ADDRESS (if different from Controlling Office)		15. SECURITY CLASS. (of this report): UNCLASSIFIED
		15a. DECLASSIFICATION/DOWNGRADING SCHEDULE

16. DISTRIBUTION STATEMENT (of this Report)

Distribution unlimited

17. DISTRIBUTION STATEMENT (of the abstract entered in Block 20, if different from Report)

18. SUPPLEMENTARY NOTES

19. KEY WORDS (Continue on reverse side if necessary and identify by block number)

Air-Sea Interaction
Mixed Layer
Ocean Forecasting

20. ABSTRACT (Continue on reverse side if necessary and identify by block number)

A one-dimensional model has been used to investigate the effect of inaccuracies in meteorological parameters on forecasts of upper ocean thermal structure. Vertical eddy fluxes of heat, salinity, and momentum in the oceanic mixed layer are parameterized using the Level-2 turbulence closure model of Mellor and Yamada (1974). Surface eddy fluxes of sensible heat, latent heat, and momentum are related to the imposed meteorological parameters through a bulk aerodynamic formulation. Surface fluxes of solar and

CONT'

DD FORM 1 JAN 73 1473 EDITION OF 1 NOV 65 IS OBSOLETE S/N 0102-LF-014-6601

UNCLASSIFIED

SECURITY CLASSIFICATION OF THIS PAGE (When Data Entered)

41

206

From Block #20

infrared radiation are parameterized with the formulas of Wyrtki (1965).

The temperature anomaly in the ocean forecast produced by inaccuracies in the meteorological parameters diffuses rapidly downward from the surface to within a few meters of the mixed layer base. Its downward diffusion is much slower below this level and this tends to produce a relatively large vertical gradient in temperature anomaly near the base of the mixed layer which may have important implications for acoustic modeling. Both the depth of the mixed layer and the magnitude of the mixed layer temperature anomaly are found to be nonlinear functions of the inaccuracies in the potential temperature, humidity, and wind speed of the atmospheric mixed layer.

Estimates of the time evolution of the inaccuracies in the air temperature, humidity, and wind speed during an actual operational forecast situation are made. For the typical summertime subtropical stratification considered here, the temperature anomalies resulting at the end of a five day forecast from these inaccuracies alone are a substantial fraction of the minimum prediction performance criterion for the Navy's Ocean Prediction System.

ACKNOWLEDGMENTS

This work was supported by the Navy under Contract N00014-78-C-0287. Contract monitor was Dr. Steve Piacsek of the Naval Ocean Research and Development Activity.

TABLE OF CONTENTS

LIST OF TABLES

LIST OF FIGURES

ABSTRACT

A one-dimensional model has been used to investigate the effect of inaccuracies in meteorological parameters on forecasts of upper ocean thermal structure. Vertical eddy fluxes of heat, salinity, and momentum in the oceanic mixed layer are parameterized using the Level-2 turbulence closure model of Mellor and Yamada (1974). Surface eddy fluxes of sensible heat, latent heat, and momentum are related to the imposed meteorological parameters through a bulk aerodynamic formulation. Surface fluxes of solar and infrared radiation are paramaterized with the formulas of Wyrtki (1965).

The temperature anomaly in the ocean forecast produced by inaccuracies in the meteorological parameters diffuses rapidly downward from the surface to within a few meters of the mixed layer base. Its downward diffusion is much slower below this level and this tends to produce a relatively large vertical gradient in temperature anomaly near the base of the mixed layer which may have important implications for acoustic modeling. Both the depth of the mixed layer and the magnitude of the mixed layer temperature anomaly are found to be nonlinear functions of the inaccuracies in the potential temperature, humidity, and wind speed of the atmospheric mixed layer.

Estimates of the time evolution of the inaccuracies in the air temperature, humidity, and wind speed during an actual operational forecast situation are made. For the typical summertime subtropical stratification considered here, the temperature anomalies resulting at the end of a five day forecast from these inaccuracies alone are a

substantial fraction of the minimum prediction performance criterion for the Navy's Ocean Prediction System.

1.0 INTRODUCTION

The sophistication of the Navy's various acoustic detection systems has increased in recent years and made detailed knowledge of the oceanic environment of prime importance. Presently, however, the Navy has no capability to forecast the internal structure of the ocean and must rely on coarse analyses of historic and synoptic data for its needs. The Naval Oceanographic Prediction System (OPS) has been proposed to provide the Navy with a better knowledge of the oceanic environment on an operational basis. The goal of OPS is to provide five-day predictions of the major features of the world ocean with reasonable accuracy and detail and two-day predictions for smaller regions with higher accuracy and detail. When it is completed, OPS will become part of the Primary Environmental Processing System (PEPS) at Fleet Numerical Weather Central. There it will interface with a data analysis and initialization system and an atmospheric prediction model to provide a dynamic description of the marine environment.

Computed ocean forecasts will be subject to error. The reasons for these forecast errors fall into three basic categories as described below.

1) The instantaneous state of the ocean is never known exactly. Thus, the initial conditions supplied to the ocean forecast model will differ from the true initial conditions.

2) The ocean forecast model cannot reproduce the internal dynamics of the ocean exactly. This is

caused primarily by the fact that the model is discrete in time and space and cannot resolve all scales of motion.

3) The state of the atmosphere and therefore the meteorological forcing of the ocean are not known exactly during the forecast period. This is because the forecast state of the atmosphere is also subject to inaccuracies, mainly resulting from inexact knowledge of initial conditions and incorrect representation of internal atmospheric dynamics. An additional source of error is that the forecast sea surface temperature, which provides important lower boundary conditions for the model atmosphere, will not be perfect.

In this paper we will investigate ocean forecast errors due to the reasons listed in category 3 above by investigating the sensitivity of 5-day forecasts to inaccuracies in cloud cover, temperature, humidity, and wind speed above the sea surface. We will restrict our attention to regions of relatively high horizontal uniformity and will concern ourselves primarily with forecasting the vertical thermodynamic structure of the upper ocean. Thus, this study can be accomplished with a one-dimensional model.

Almost universally, the upper ocean is characterized by a mixed layer extending from the surface to about 5-100 m depth in which temperature, salinity, and current velocity exhibit only a very small change with depth. This layer owes its high degree of vertical homogeneity to mixing caused by turbulence that is generated by the wind and intermittent

upward buoyancy flux through the sea surface. A dynamically stable water mass in which the vertical eddy fluxes are very small exists below the mixed layer. During periods of relatively strong wind forcing and/or strong surface cooling, the mixed layer tends to deepen because the more dense water from below is entrained into the layer by turbulence at its base. During periods of relatively weak wind forcing and/or strong surface heating, however, the source of turbulent kinetic energy may become too weak to maintain active entrainment at the mixed layer base, causing the layer to retreat to a shallower depth. Thus, the problem of modeling the upper ocean is closely associated with parameterization of turbulent processes in the mixed layer.

The first attempts at modeling the upper ocean were with diffusive models. In this type of approach, vertical turbulent fluxes are parameterized in terms of the mean fields using eddy diffusion coefficients which may themselves depend on the mean fields. An advantage of this type of model is that no assumptions (other than the eddy coefficient assumption) need to be made concerning the behavior of the mixed layer.

The first diffusive model that predicted the density and current structure of the upper ocean was that of Munk and Anderson (1948). The forms of the eddy coefficients in this model were determined empirically from stratified turbulence data. Mamayev (1958) and Pandolfo (1969) have also proposed empirical forms for the eddy diffusion coefficients. More recently, models such as those of Vager and Zilitinkevich (1968) and Mellor and Yamada (1974) have been developed in light of modern turbulence closure theory. Martin (1976) and Jacobs (1978) have performed numerical experiments comparing several of the proposed forms of the eddy coefficients.

We will use the diffusive (i.e., Level 2) model of Mellor and Yamada (1974) in this study. This model has been applied to the upper ocean with good success by Mellor and Durbin (1975). Martin (1976) concluded that it was the most suitable model for simulating the upper ocean among those he compared and it has been proposed as an important component of OPS (Grabowski and Roberts, 1978).

We will parameterize the surface eddy fluxes of latent and sensible heat using the bulk aerodynamic method in which the fluxes are related to mean field quantities by means of bulk exchange coefficients. This technique is based primarly on the theory of Monin and Obukhov (1954) and has been reviewed comprehensively by Businger (1975) and Busch (1977).

The remainder of this paper is organized as follows: Section 2 describes the model ocean. Section 3 discusses the parameterization of the surface fluxes. Section 4 describes the design of the experiments. Section 5 presents the results. Section 6 is a summary.

2.0 DESCRIPTION OF THE MODEL OCEAN

2.1 Fundamental Equations

Assuming zero mean vertical motion and horizontal uniformity for all fields, the conservation equations for heat, salt, and momentum in the upper ocean can be written

$$\frac{\partial \bar{T}}{\partial t} = \frac{\partial}{\partial z}\left(K_H \frac{\partial \bar{T}}{\partial z}\right) + \frac{1}{\rho_w c} \frac{\partial F}{\partial z} \tag{1}$$

$$\frac{\partial \bar{S}}{\partial t} = \frac{\partial}{\partial z}\left(K_S \frac{\partial \bar{S}}{\partial z}\right) \tag{2}$$

$$\frac{\partial \bar{\underset{\rightarrow}{v}}}{\partial t} = f\,\hat{k} \times \bar{\underset{\rightarrow}{v}} + \frac{\partial}{\partial z}\left(K_M \frac{\partial \bar{\underset{\rightarrow}{v}}}{\partial z}\right) \tag{3}$$

where T is the temperature, S the salinity, $\underset{\rightarrow}{v}$ the horizontal current velocity vector (standard right-handed Cartessian coordinate system with z positive upward and origin at sea surface assumed), F the downward flux of solar radiation, and f the Coriolis parameter. Other symbols are defined in the Appendix and all the notation is standard. Spatial averages

at constant depth taken across a region large enough to encompass a statistically significant sampling of all unresolved phenomena are denoted by $(^-)$ and implicit in (1)-(3) are the eddy coefficient assumptions

$$\overline{w'T'} = -K_H \frac{\partial \bar{T}}{\partial z} \tag{4}$$

$$\overline{w'S'} = -K_S \frac{\partial \bar{S}}{\partial z} \tag{5}$$

$$\overline{w'\underset{\sim}{Y}'} = -K_M \frac{\partial \bar{\underset{\sim}{Y}}}{\partial z} \tag{6}$$

where w is the vertical component of the motion, and the primes indicate departures from the horizontal averages. The quantities K_H, K_S, and K_M are the eddy diffusion coefficients and are determined from the considerations in the next section. Finally, we note that all horizontal eddy fluxes are assumed zero.

2.2 Determination of the Eddy Diffusion Coefficients

Through systematic scaling of the equations for the Reynolds fluxes and turbulent kinetic energy, Mellor and

Yamada (1974) developed a set of turbulence closure models for planetary boundary layers labeled, in order of increasing complexity, Levels 1 through 4. They used hypotheses proposed by Kolmogoroff (1942) and Rotta (1951) to model the triple correlation and dissipation terms in these equations and the empirical constants arising from the theory were determined from neutrally stratified turbulence data.

In the Level 2 model, which will be used here, (4)-(6) are recovered with the eddy diffusion coefficients given by

$$K_H = l(2\bar{E})^{\frac{1}{2}} A_H \tag{7}$$

$$K_M = l(2\bar{E})^{\frac{1}{2}} A_M \tag{8}$$

where l is a turbulence length scale and $\bar{E}$ is the turbulent kinetic energy

$$\bar{E} = \tfrac{1}{2}\overline{(u'^2 + v'^2 + w'^2)} \tag{9}$$

The quantities A_H and A_M are stability functions given by

$$A_H = n_1 - \frac{n_2 R_f}{(1-R_f)} \tag{10}$$

$$A_M = \frac{A_H \left(n_3 - \dfrac{n_4 R_f}{(1-R_f)}\right)}{\left(n_5 - \dfrac{n_6 R_f}{(1-R_f)}\right)} \tag{11}$$

where the n_1-n_6 are empirical constants and

$$R_f = \frac{A_H}{A_M} \left[\frac{g}{\rho_w} \frac{\partial \bar{\rho}}{\partial z} \left| \frac{\partial \bar{\vec{V}}}{\partial z} \right|^{-2} \right] \tag{12}$$

Note here that the mean field density $\bar{\rho}$ in (12) can be related to the mean field temperature and salinity with a linearized equation of state

$$\bar{\rho} = \rho_w \left| 1 - a(\bar{T} - T_w) + b(\bar{S} - S_w) \right| \tag{13}$$

where ρ_w is a reference density, T_w a reference temperature, S_w a reference salinity and a and b empirical constants. Note also that, following many others, we assume

$$K_S = K_H \tag{14}$$

The turbulent kinetic energy $\bar{E}$ is calculated from

$$0 = K_M \left| \frac{\partial \vec{v}}{\partial z} \right|^2 - K_H g \left[a \frac{\partial \bar{T}}{\partial z} - b \frac{\partial \bar{S}}{\partial z} \right] - n_7 \bar{E}^{3/2} \tag{15}$$

The three terms on the right of (15) represent shear production, buoyant damping, and viscous dissipation of turbulent kinetic energy respectively.

Finally, an estimate of the turbulence length scale l is calculated from the vertical extent of the turbulence field according to

$$l = \frac{n_8 \int_{-\infty}^{0} z\bar{E}^{\frac{1}{2}}\, dz}{\int_{-\infty}^{0} \bar{E}^{\frac{1}{2}}\, dz} \tag{16}$$

which closes the model.

Note that the "mixed layer" is henceforth defined as the region where $\bar{E}>0$. Below the mixed layer we retain weak vertical diffusion by setting

$$K_H = K_S = K_M = 1 \text{ cm}^2 \text{ s}^{-1} \tag{17}$$

For a detailed discussion of the scaling which leads to this turbulence closure theory, see Mellor and Yamada (1974).

3.0 PARAMETERIZATION OF THE SURFACE FLUXES

The total fluxes of heat, salinity, and momentum at the ocean surface are given by

$$\rho_w c\overline{(w'T')}_o = F_o + B_o + H_o + L_v Q_o \tag{18}$$

$$\rho_w\overline{(w'S')}_o = S_o(P_o - Q_o) \tag{19}$$

$$\rho_w\overline{(w'\underset{\rightarrow}{v}')}_o = -\underset{\rightarrow}{\tau}_o \tag{20}$$

where F is the total solar radiation flux, B the infrared radiation flux, H the sensible heat flux, L_vQ the latent heat flux, P the precipitation rate and $\underset{\rightarrow}{\tau}$ the wind stress vector. The subscript o indicates evaluation of quantities at the sea surface and all fluxes are taken positive upward. Note that implicit in (20) is the assumption of a fully-developed sea.

The surface fluxes of sensible heat, latent heat, and momentum can be related to mean field quantities using the Monin-Obukhov theory (see Busch, 1977)

$$H_o = \rho_a c_p C_\theta(\bar{U}_r-\bar{U}_o)(\bar{\theta}_o-\bar{\theta}_r) \tag{21}$$

$$L_vQ_o = \rho_a L_v C_q(\bar{U}_r-\bar{U}_o)(\bar{q}_o-\bar{q}_r) \tag{22}$$

$$\underset{\rightarrow}{\tau}_o = \rho_a C_m(\bar{U}_r-\bar{U}_o)^2 \frac{\underset{\rightarrow}{V}_r}{|\underset{\rightarrow}{\bar{V}}_r|} \tag{23}$$

where U is wind speed, $\underline{V}$ is wind velocity, θ is potential temperature of the air, and q is water vapor mixing ratio (mass of water vapor per mass of dry air). The subscript r indicates evaluation of quantities at some reference level z_r and the subscript o indicates evaluation of quantities at the sea surface. A reference density for air is denoted by ρ_a and c_p is the specific heat at constant pressure for air.

The C_α in (21)-(23) are bulk aerodynamic drag coefficients defined by

$$C_\alpha = \frac{\kappa^2}{\left[\ln \frac{z_r}{z_{o\alpha}} - \Psi_\alpha\right]\left[\ln \frac{z_r}{z_o} - \Psi_m\right]}, \alpha = \theta, q, m \qquad (24)$$

where κ is vonKarmen's constant, $z_{o\alpha}$ and z_o are surface roughness lengths, and the Ψ_α are defined by

$$\Psi_\alpha = \int_o^{z_r/L} \frac{1 - \phi_\alpha(\xi)}{\xi} d\xi, \quad \alpha = \theta, q, m \qquad (25)$$

with ϕ_α non-dimensional gradients given by

$$\phi_\theta = \frac{\rho_o c_p u_* \kappa z}{H_o} \frac{\partial \bar{\theta}}{\partial z} \qquad (26)$$

$$\phi_q = \frac{\rho_o u_* \kappa z}{Q_o} \frac{\partial \bar{q}}{\partial z} \tag{27}$$

$$\phi_m = \frac{\kappa z}{u_*} \frac{\partial \bar{U}}{\partial z} \tag{28}$$

and u_* the surface friction velocity in the air defined by

$$u_* = \left(\frac{|\vec{\tau}_o|}{\rho_a} \right)^{\frac{1}{2}} \tag{29}$$

The quantity L in (25) is the Monin-Obukhov stability length, given to good approximation by

$$L = \frac{-\rho_a u_*^3}{\kappa g \left[\frac{H_o}{c_p T_o} + 0.61 Q_o \right]} \tag{30}$$

Over most of the ocean, the usual situation is one of upward surface fluxes of sensible and latent heat which implies $L<0$. In this case an atmospheric mixed layer in which $\bar{\theta}$, $\bar{q}$, and $\bar{\underset{\rightarrow}{V}}$ are relatively homogeneous is observed to exist extending from the top of the surface layer (at a height of $-L$) to several hundred meters altitude.

Eventually and in support of OPS, satellites will routinely supply observations of mixed layer values for potential temperature, water vapor mixing ratio, and wind velocity over much of the ocean. Thus, it is appropriate in this study to relate the surface fluxes to mean field quantities characteristic of the atmospheric mixed layer, which can be done by taking $z_r=-L$.

Monin-Obukhov similarity theory predicts that the non-dimensional gradient functions ϕ_α will be functions of only z/L in the atmospheric surface layer. Proposed forms of the ϕ functions have been reviewed by Hogstrom (1974) and it is generally accepted that most surface layer data are well represented by

$$\left.\begin{aligned} \phi_\theta &= \phi_q = (1 - 9\,\frac{z}{L})^{-\frac{1}{2}} \\ \phi_m &= (1 - 15\,\frac{z}{L})^{-\frac{1}{4}} \end{aligned}\right\} \quad \text{for } L < 0 \qquad (31)$$

which are the forms used here. Thus, making use of the fact that H_o, Q_o, and $\underset{\rightarrow}{I}_o$ are approximately constant in the

atmospheric surface layer, setting z_r=-L, and using (24), (25), and (31), the bulk aerodynamic coefficients can be written

$$C_\theta = C_q = \frac{\kappa^2}{\left[\ln\left(\frac{-L}{z_o}\right) - 1.466\right]\left[\ln\left(\frac{-L}{z_o}\right) - 0.844\right]} \tag{32}$$

$$C_m = \frac{\kappa^2}{\left[\ln\left(\frac{-L}{z_o}\right) - 0.844\right]^2} \tag{33}$$

where, following many others we have assumed

$$z_{o\alpha} = z_o \quad \alpha = \theta, q, m \tag{34}$$

Furthermore, following Clarke (1970) we assume

$$z_o = \max\left(\frac{0.032u_*^2}{g}, z_{min}\right) \tag{35}$$

were z_{min}=0.0015 cm. We set θ_o equal to the temperature at the uppermost gridpoint of the model ocean and thus neglect any skin temperature effects (see Grassl, 1976). We

set q_o equal to the saturation value at the sea surface and for simplicity we take U_o equal to zero and assume that the surface stress vector is in the direction of the mixed layer wind velocity. Furthermore, since we have set $z_r=-L$, $\bar{\theta}_r, \bar{q}_r$, and $\bar{U}_r$ are given to excellent approximation by the values of these quantities characteristic of the atmospheric mixed layer θ_m, q_m, and U_m. Thus, having specified θ_m, q_m, and $\underset{\sim}{V}_m$ (here $\underset{\sim}{V}_m$ is the wind velocity vector characteristic of the atmospheric mixed layer), (21)-(23), (30), (32), (33), and (35) can be solved iteratively to yield H_o, $L_v Q_o$, and $\underset{\sim}{\tau}_o$.

Finally we calculate the surface radiative fluxes using the expressions presented by Wyrtki (1965)

$$F_o = F_i \left|1 - 0.38(C+C^2)\right| \tag{36}$$

$$B_o = \varepsilon b_* T_o^4 (0.39 - 2.0\, q_{10}^{\frac{1}{2}})(1 - 0.56C^2) + 4\varepsilon b_* T_o^3 (T_o - T_{10}) \tag{37}$$

where F_i is the surface solar flux in the absence of clouds, C is the fractional cloud cover, ε the infrared emissivity of the sea surface, b_* the Stefan-Boltzmann constant, T_o the sea surface temperature, T_{10} the air temperature at 10 m height, and q_{10} the water vapor mixing ratio at 10 m height. Since the surface layer will be thicker than 10 m for all cases considered here (i.e., $-L>10$ m), T_{10} and q_{10} can be determined by using (31) and integrating the profile relations (26) and (27) from the surface to the 10 m height.

4.0 DESCRIPTION OF THE EXPERIMENTS

To investigate the effect of inaccuracies in the meteorological parameters (θ_m, q_m, U_m, C) on a one-dimensional forecast of upper ocean thermal structure, a set of 11 experiments are performed. The initial conditions are the same for all experiments, characteristic of the summertime subtropical ocean, and given in Table 1. The imposed meteorological parameters vary from experiment to experiment, however, and are summarized in Table 2. All model integrations are carried out five days.

The Control Experiment (see Table 2) can be thought of as a special case in which the meteorological parameters are known exactly during the course of the integration. The predictions for the other experiments will be regarded as those resulting when the meteorological parameters are not known exactly during the forecast period. Thus, anomalies between the predicted thermal structure for the Control Experiment and the remaining experiments give measures of the errors in the ocean predictions resulting from various inaccuracies ($\Delta\theta_m$, Δq_m, etc.) in the meteorological parameters.

Experiments 1-8 are designed to illustrate the model's response to changes in the meteorological parameters of standard magnitude (i.e., 1°C, 1 gm kg^{-1}, etc.). Thus, for this subset of the experiments, these quantities are varied one at a time and held constant during the forecast period.

In Experiments 9 and 10 we simulate a more realistic forecast situation by allowing the inaccuracies to occur in

TABLE 1

Initial Conditions for
all Experiments

$z(m)$	$\bar{T}(^{o}C)$	$\bar{S}(o/oo)$	$\bar{\vec{v}}(ms^{-1})$
$0 \geq z \geq -20$	27.65	35	$-0.12\hat{j}$
$-20 > z \geqslant -60$	$27.65+(z+20)(0.025)$	35	0

TABLE 2

SUMMARY OF EXPERIMENTS

$\theta_m = (26 + \Delta\theta_m)^{o}C$

$q_m = (17.5 + \Delta q_m)gm\ kg^{-1}$

$\underset{\rightarrow}{V}_m = -(8 + \Delta U_m)\ m\ s^{-1}\ \hat{i}$

$C = (0.1 + \Delta C)$

Experiment	$\Delta\theta_m$ (^{o}C)	Δq_m ($gm\ kg^{-1}$)	ΔU_m (ms^{-1})	ΔC
Control	0	0	0	0
1	-1	0	0	0
2	0	-1	0	0
3	0	0	1	0
4	0	0	0	0.1
5	1	0	0	0
6	0	1	0	0
7	0	0	-1	0
8	0	0	0	-0.1
9	$-0.187(1+1.27\ day^{-1}t)$	$-0.2(1+1.27\ day^{-1}t)$	$0.312(1+1.27\ day^{-1}t)$	0
10	$0.187(1+1.27\ day^{-1}t)$	$0.2(1+1.27\ day^{-1}t)$	$-0.312(1+1.27\ day^{-1}t)$	0

several meteorological parameters simultaneously and grow with time. The inaccuracies increase during the course of the integration because the errors in the atmospheric forecast will grow with time. A discussion of the relevance of the assumed inaccuracies for the meteorological parameters in Experiments 9 and 10 can be found in section 5.2.

Finally, we note that values for the empirical constants n_1-n_8 in the turbulent diffusion model are those given by Mellor and Yamada (1974). All other consants can be found either in standard reference books or Table 3. The numerical scheme used is forward in time with the diffusive terms in (1)-(3) treated implicitly. A uniform grid with a spacing of 2 m extending from the surface to a depth of 60 m is used. The absorption of solar radiation in (1) is modeled using the Type I extinction profile from Jerlov (1951).

TABLE 3

Model Constants and Parameters

Quantity	Symbol	Value
Coriolis parameter	f	6.73×10^{-5} s^{-1}
daily-averaged downward flux of solar radiation at sea surface for cloudless conditions	F_i	575 ly day^{-1}
von Karman's constant	κ	0.4

5.0 RESULTS

5.1 Model Response to Constant Inaccuracies in the Meteorological Parameters

In this section we present results from Experiments 1-8 in the form of time-depth contours of temperature anomaly between the experiment in question and the Control Experiment. These temperature anomalies can be regarded as errors in the ocean forecast resulting from the constant prescribed inaccuracies in the various meteorological parameters ($\Delta\theta_m$, Δq_m, etc.) summarized in Table 2.

Fig. 1 shows the results for Experiment 1 ($\Delta\theta_m$=-1°C). The -2 contour line correponds closely with the base of the mixed layer and anomalously cool water, caused primarily by an increased flux of sensible heat from sea to air, exists in the mixed layer. As will be the case for all the experiments, the temperature anomaly diffuses rapidly downward from the surface to within a few meters of the mixed layer base, where its downward diffusion becomes much slower. This is due to the rapid decrease in turbulent kinetic energy (and, consequently, eddy diffusivity) with depth near the base of the mixed layer.

Note the relatively large vertical gradient in temperature anomaly at the base of the mixed layer near the end of the five day forecast (see Fig. 1). This result will also appear in the other experiments and may be significant since the vertical temperature gradient near the mixed layer base is an important quantity in the theory of underwater sound propagation.

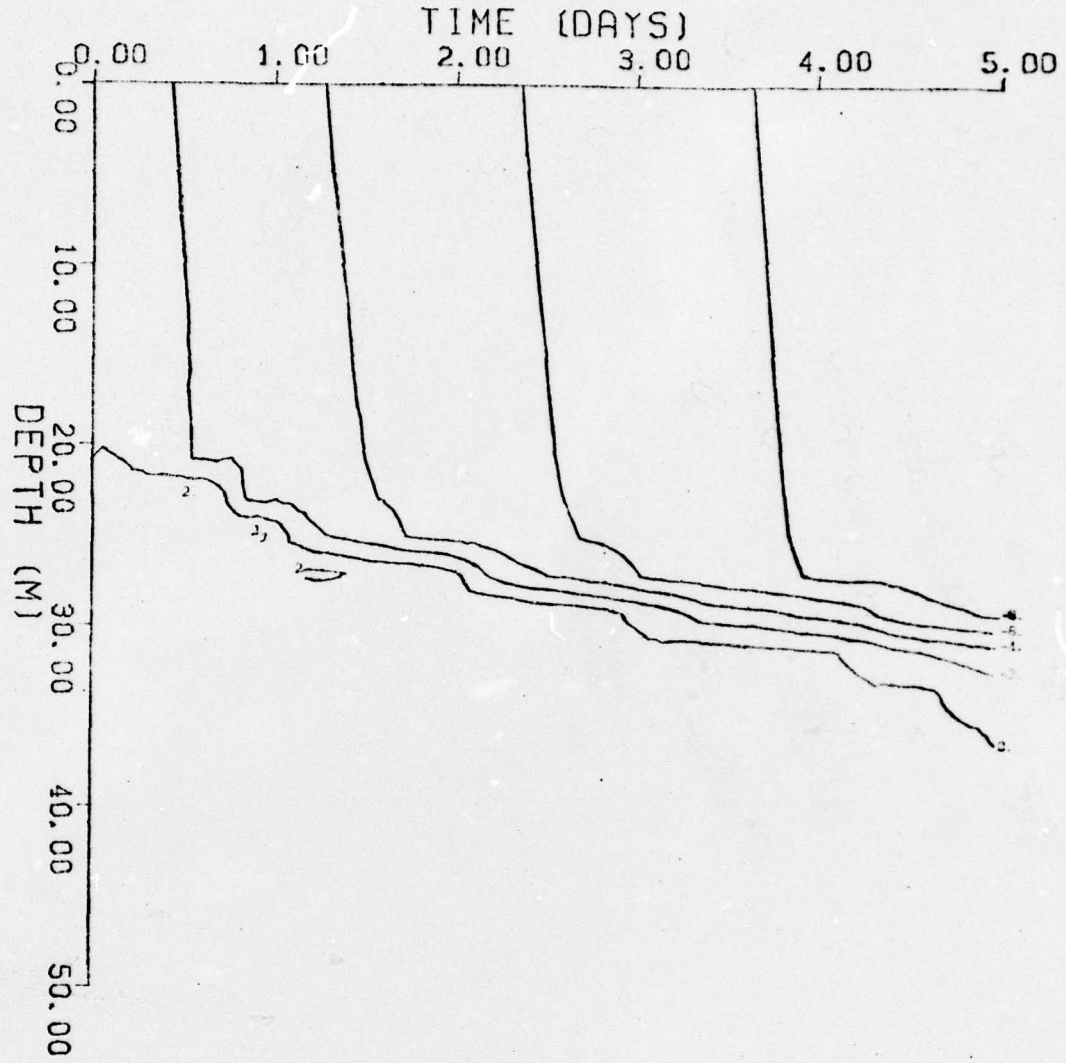

Figure 1. Time-depth contours of temperature in Experiment 1 ($\Delta\theta_m = -1\ ^oC$, $\Delta q_m = 0$, $\Delta U_m = 0$, $\Delta C = 0$) minus temperature in the control Experiment. Contour units are $10^{-2}\ ^oC$.

Also of interest in Fig. 1 is the fact that the magnitude of the temperature anomaly in the mixed layer increases more rapidly near the beginning of the five day forecast than near the end. This occurs, primarily, because the mixed layer deepens during the period and, consequently, its thermal inertia is larger near the end of the experiment.

Fig. 2 shows the results for Experiment 2 (Δq_m=-1 gm kg^{-1}). In this case, the anomalously cool water in the mixed layer is due primarily to an increased flux of latent heat from sea to air. Comparison of Fig. 1 and Fig. 2 indicates remarkable qualitative similarity. The base of the mixed layer for Experiment 2 is again well determined by the -2 contour. Therefore, Figs. 1 and 2 show that the time evolution of the mixed layer depth is very similar for both Experiments 1 and 2. Note, however, that the mixed layer temperature anomaly grows about 10% faster for Experiment 2 than for Experiment 1.

Fig. 3 shows the results for Experiment 3 (ΔU_m=1 m s^{-1}). Increased surface fluxes of both sensible and latent heat in this case are primarily responsible for producing anomalously cool water in the mixed layer. Note, however, that the temperature anomaly in the mixed layer grows slower in this experiment than in either Experiments 1 or 2.

After day 1, the mixed layer is generally a few meters deeper in Experiment 3 than in the previous two experiments. In addition, an anomalous quasi-periodic fluctuation in mixed layer depth with an amplitude of about 1 m, which was not present in the previous two experiments, is superimposed on the slow deepening rate of the mixed layer in this

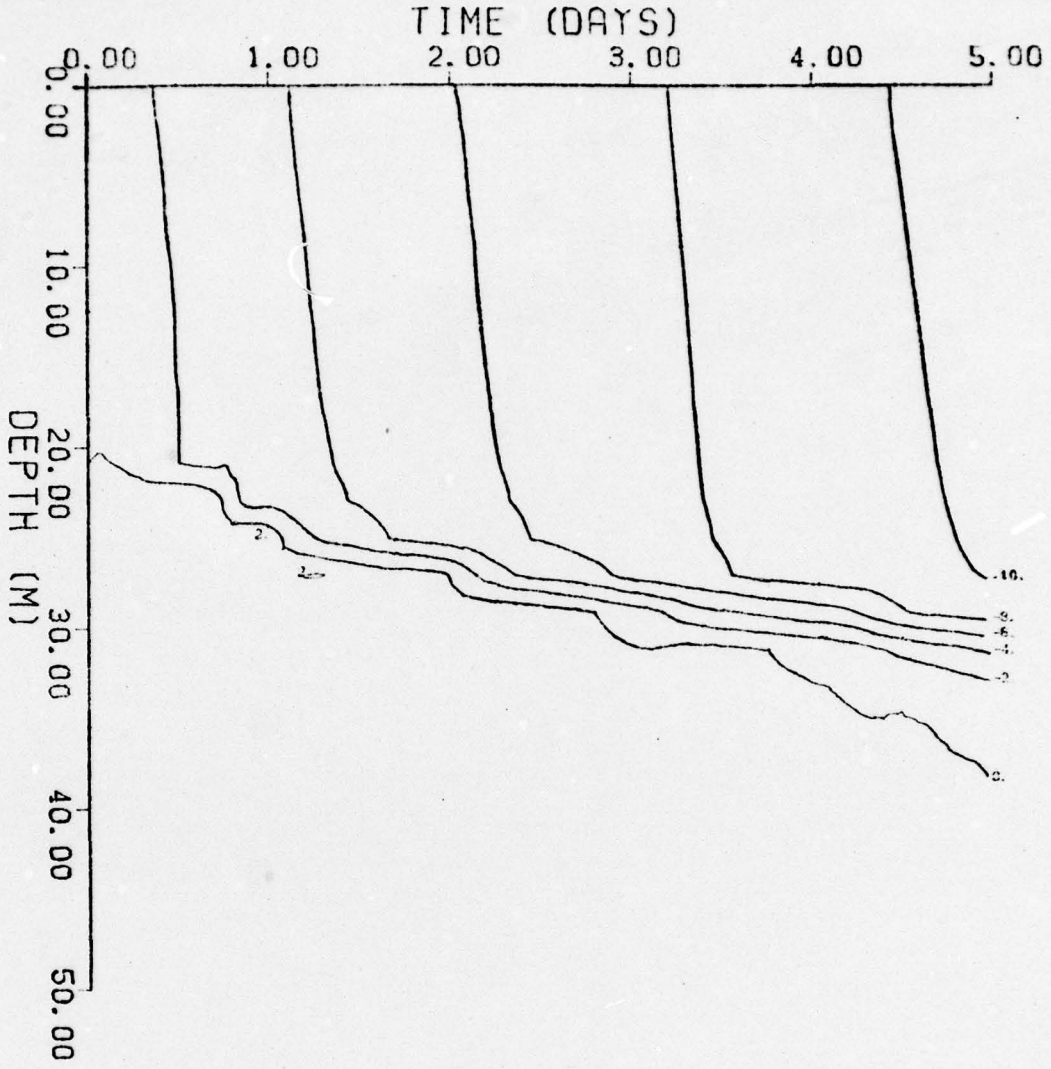

Figure 2. Same as Figure 1 but for Experiment 2 ($\Delta\theta_m = 0$, $\Delta q_m = -1$ gm kg^{-1}, $\Delta U_m = 0$, $\Delta C = 0$).

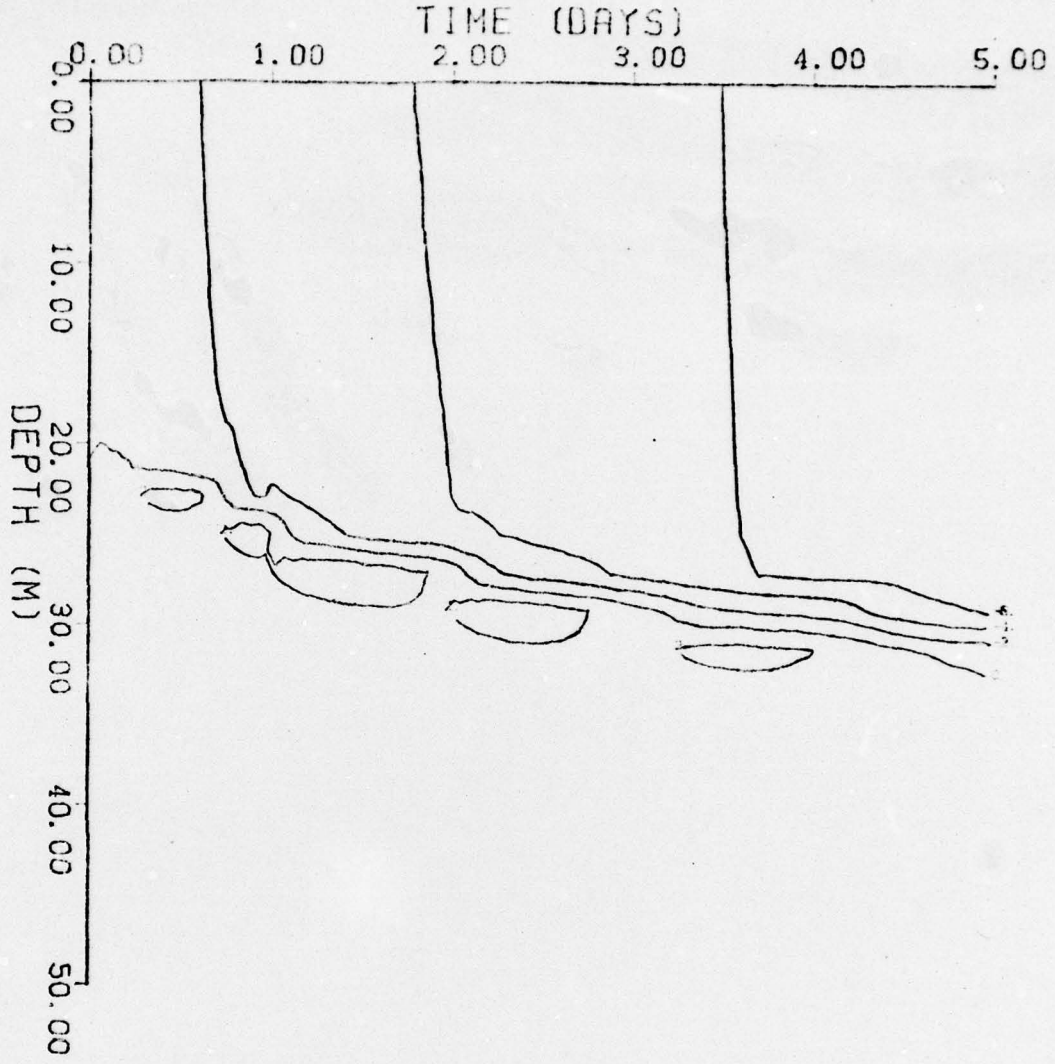

Figure 3. Same as Figure 1 but for Experiment 3 ($\Delta\theta_m = 0$, $\Delta q_m = 0$, $\Delta U_m = 1\ m s^{-1}$, $\Delta C = 0$).

experiment. This anomalous fluctuation in mixed layer depth produces the quasi-periodic variation in temperature anomaly near the base of the layer evident in Fig. 3.

The fluctuation in mixed layer depth is associated with the flux of wind energy from air to sea which is given by the dot product of the surface wind stress vector and the surface current velocity vector, $\underset{\sim}{\tau}_o \cdot \bar{\underset{\sim}{v}}_o$. Although the wind stress vector is essentially time invariant in this experiment, the surface current velocity vector oscillates with the inertial period. Thus $\underset{\sim}{\tau}_o \cdot \bar{\underset{\sim}{v}}_o$ and, consequently, the wind generation of turbulent kinetic energy also varies with the inertial period. Since the wind speed and, therefore, the magnitude of the surface wind stress vector is larger in Experiment 3 than in the Control Experiment, an anomalous component is introduced in the inertial fluctuation of wind generation of turbulent kinetic energy. This causes the anomalous variation in mixed layer depth.

Fig. 4 shows the results for Experiment 4 ($\Delta C=0.1$). As expected, the slightly increased cloudiness produces a cool anomaly in the mixed layer. However, the magnitude of the anomaly produced is much smaller than that resulting from any of the three previous experiments.

Fig. 5 shows the results for Experiment 5 ($\Delta\theta_m=1^oC$). The warm anomaly in the mixed layer is, in this case, caused primarily by a decreased flux of sensible heat from sea to air. Comparison of Fig. 5 to Fig. 1 shows that the rate at which the magnitude of the mixed layer temperature anomaly increases is faster in Experiment 5 than in Experiment 1. Thus, the response of the mixed layer temperature anomaly to

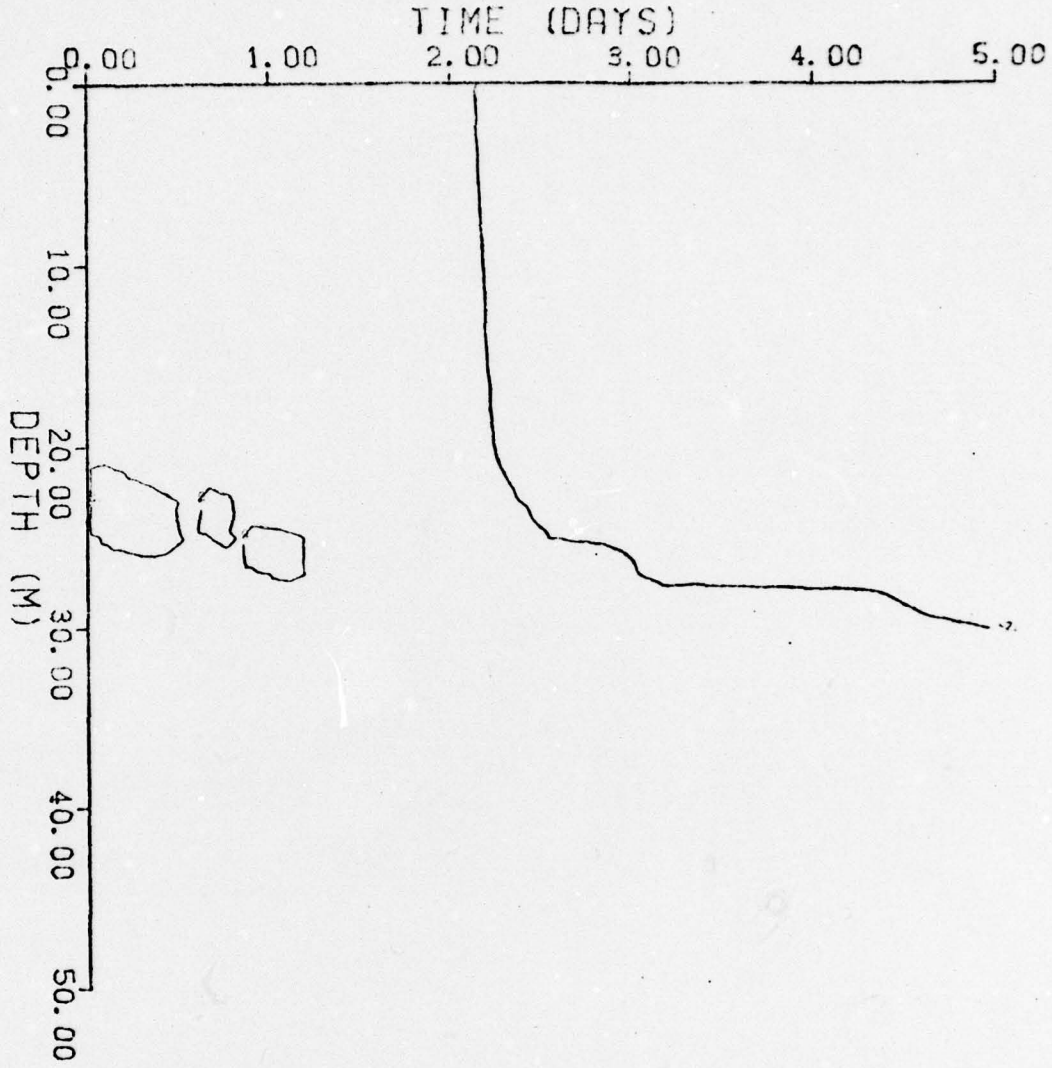

Figure 4. Same as Figure 1 but for Experiment 4 ($\Delta\theta_m = 0$, $\Delta q_m = 0$, $\Delta U_m = 0$, $\Delta C = 0.1$).

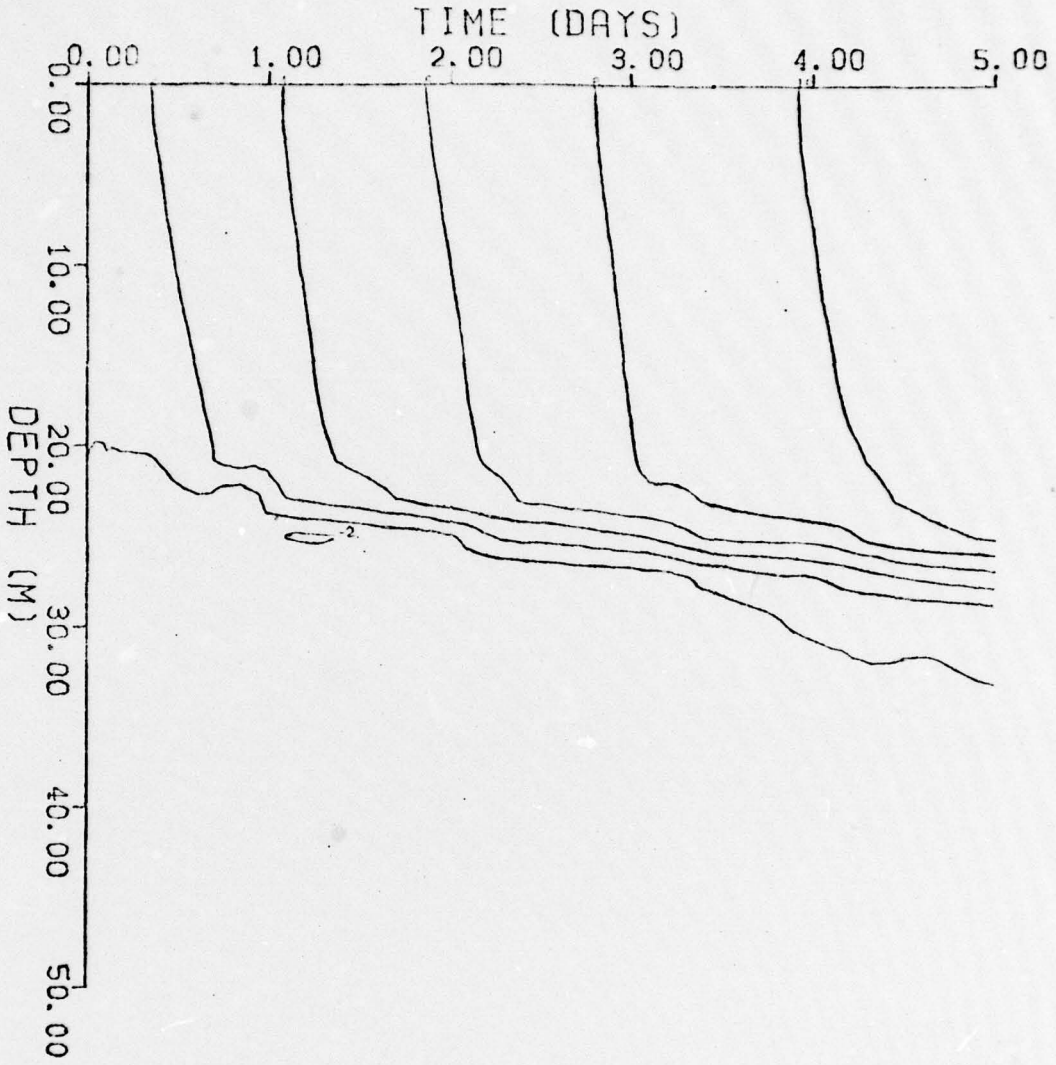

Figure 5. Same as Figure 1 but for Experiment 5 ($\Delta\theta_m$ = 1 °C, Δq_m = 0, ΔU_m = 0, ΔC = 0).

$\Delta\theta_m$ is nonlinear. This is caused partly by the fact that the mixed layer does not deepen as rapidly in Experiment 5 as it does in Experiment 1. For example, at the end of the five day period, the mixed layer is 32 m deep in Experiment 1 but only 26 m deep in Experiment 5. Thus, more cold water is entrained into the mixed layer from below in Experiment 1 than in Experiment 5. In addition, the average thermal inertia of the mixed layer is greater in Experiment 1 than in Experiment 5 since its average depth is greater.

The dependence of the drag coefficient on static stability of the atmospheric surface layer also contributes to the nonlinear response mentioned above. Specifically, the drag coefficient for latent and sensible heat in Experiment 5 is, on the average, about 15% smaller than that of Experiment 2. This models the fact that the more statically stable atmospheric stratification in Experiment 5 tends to reduce the intensity of the turbulence in the lower atmosphere.

Fig. 6 shows the results for Experiment 6 (Δq_m=1 gm kg^{-1}). The warm anomaly in the mixed layer evident in Fig. 6 is caused primarily by a decreased flux of latent heat from sea to air. Comparison of Fig. 6 to Fig. 2 indicates that the response of the mixed layer temperature anomaly to Δq_m is also nonlinear. However, the nonlinearity is not as large in this case as it was for $\Delta\theta_m$. This is because the drag coefficient for latent and sensible heat is not as sensitive to Δq_m as it is to $\Delta\theta_m$ and is only about 2% smaller in Experiment 6 than in Experiment 2. Thus, the nonlinearity here is essentially due only to the difference in deepening rate of the mixed layer between Experiments 2 and 6. The mixed layer depth in Experiment 6 behaves almost

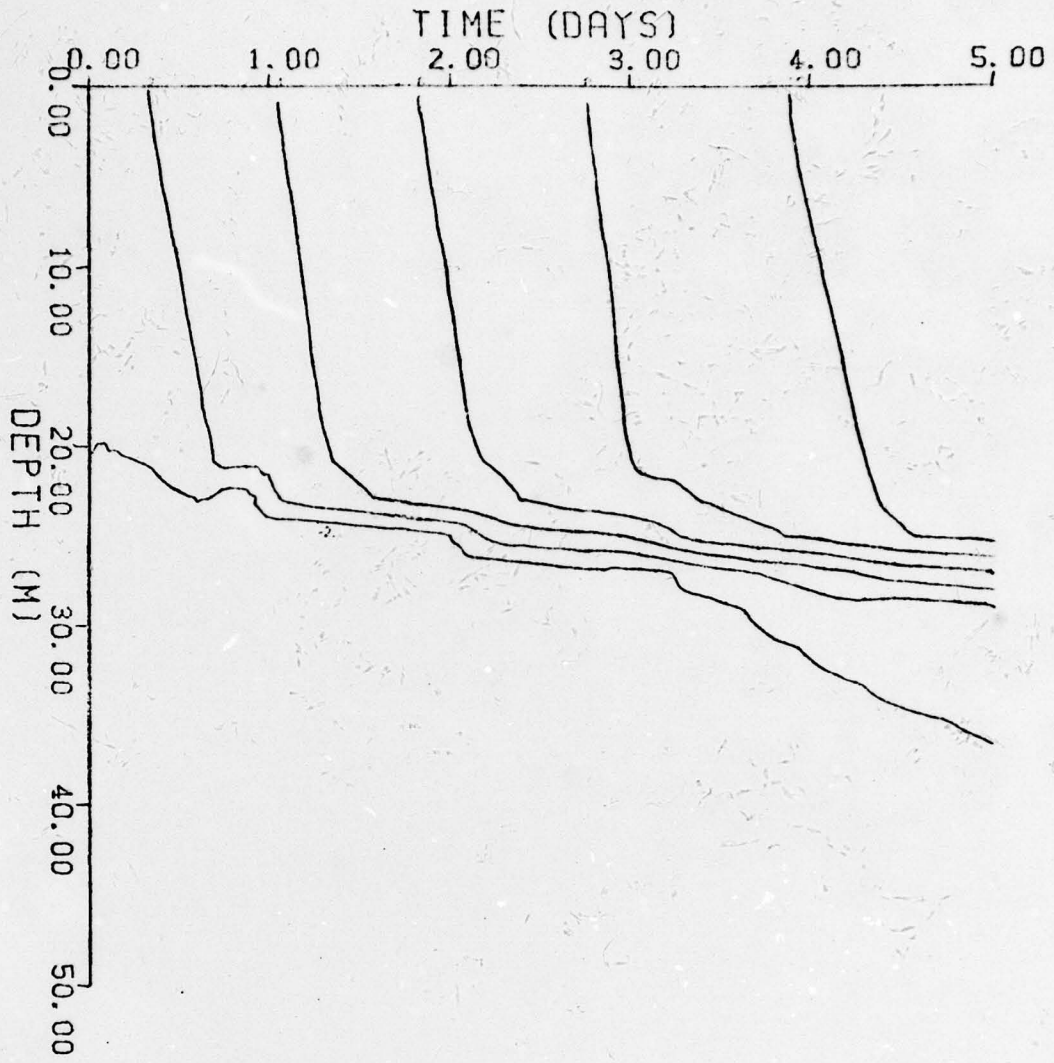

Figure 6. Same as Figure 1 but for Experiment 6 ($\Delta\theta_m = 0$, $\Delta q_m = 1$ gm kg^{-1}, $\Delta U_m = 0$, $\Delta C = 0$).

exactly the same as that of Experiment 5. Thus, at the end of the five day forecast, the mixed layer depth for Experiment 6 is only about 26 m while that of Experiment 2 is 32 m.

Fig. 7 shows the results for Experiment 7 (ΔU_m=-1 m s^{-1}). The warm anomaly present in the mixed layer in this case is due primarily to a decreased flux of both sensible and latent heat from sea to air. Not surprisingly, comparison of Fig. 7 to Fig. 3 indicates that the response of mixed layer temperature anomaly to ΔU_m is also nonlinear. As was the case for the previous experiment, this nonlinearity is due almost entirely to differences in mixed layer depth with differences in the drag coefficient playing a negligible role. Note that, after the five day forecast, the mixed layer is 32 m deep in Experiment 3 but only 26 m deep in Experiment 7.

Also of interest in Fig. 7 is the quasi-periodic variation in temperature anomaly near the base of the mixed layer. This is a result of the same mechanism discussed previously in connection with the quasi-periodic fluctuation in temperature anomaly evident in Fig. 3.

Fig. 8 shows the results for Experiment 8 (ΔC=-0.1). The warm anomaly in the mixed layer is due to the increased downward flux of solar radiation at the surface. However, as was the case for Experiment 4, the magnitude of the anomaly is small compared to that of the other experiments.

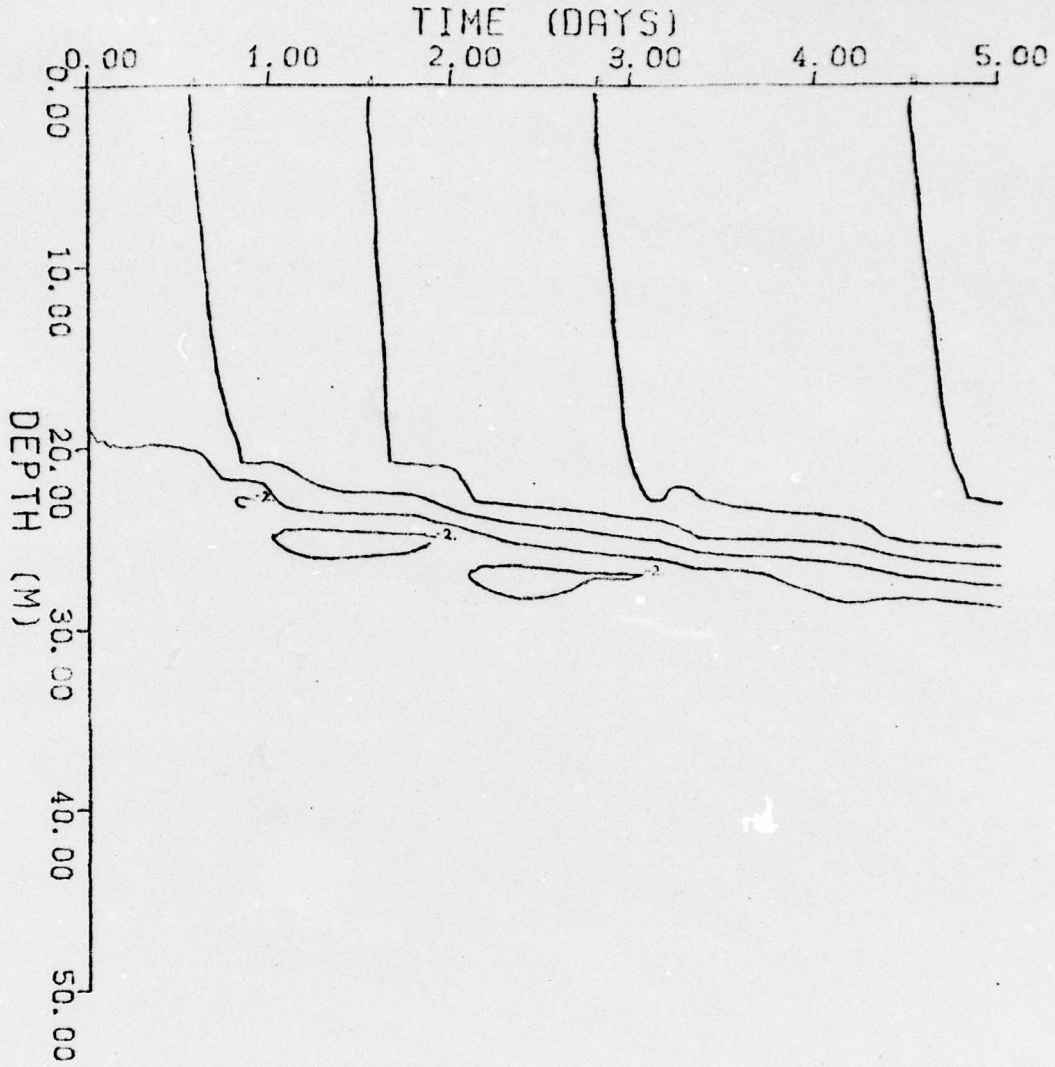

Figure 7. Same as Figure 1 but for Experiment 7 ($\Delta\theta_m = 0$, $\Delta q_m = 0$, $\Delta U_m = -1\ m\ s^{-1}$, $\Delta C = 0$).

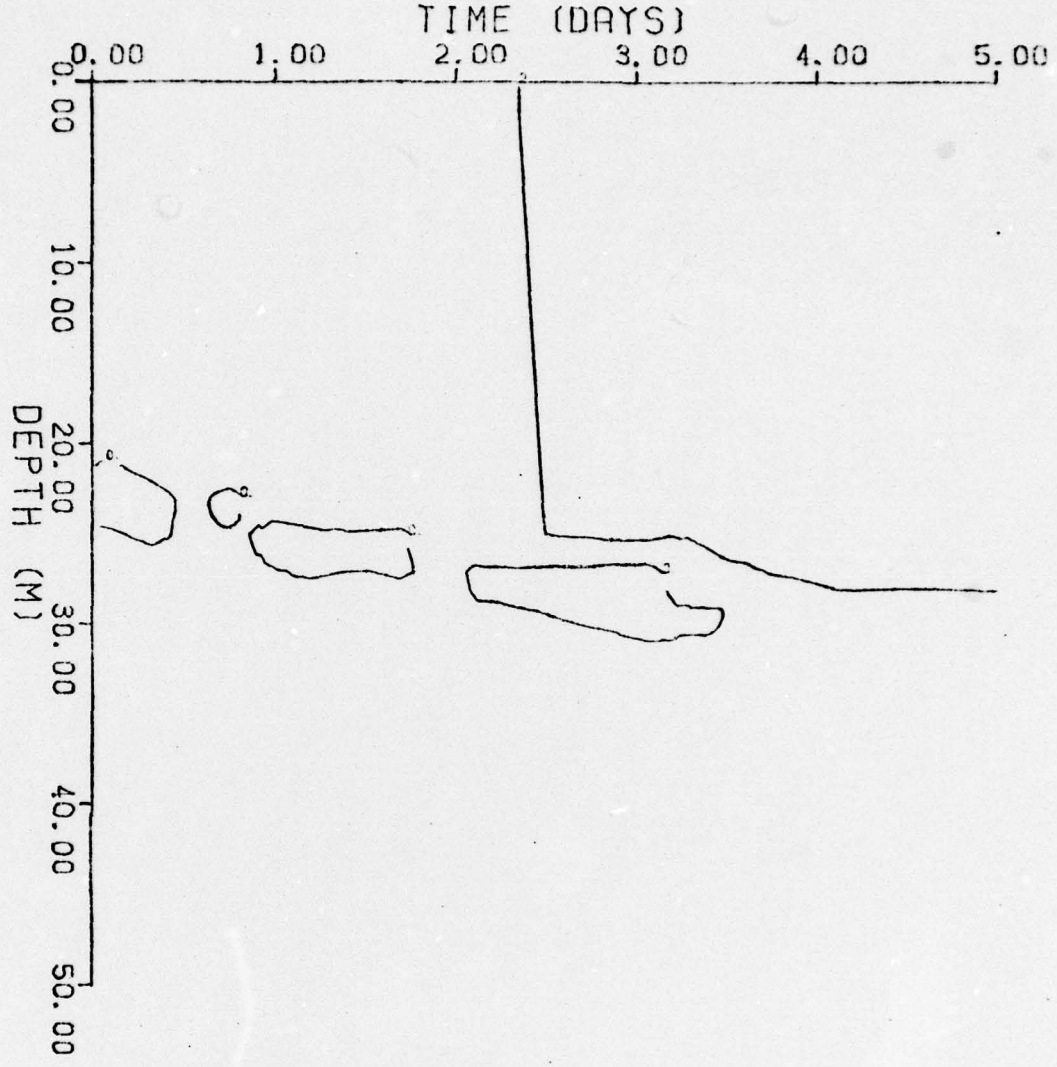

Figure 8. Same as Figure 1 but for Experiment 8 ($\Delta\theta_m = 0$, $\Delta q_m = 0$, $\Delta U_m = 0$, $\Delta C = -0.1$).

5.2 Model Response to Time-Varying Inaccuracies in the Meteorological Parameters

In this section we will investigate the model's response when the inaccuracies in the meteorological parameters vary in a manner that simulates an actual operational forecast situation.

At the beginning of the forecast period, we assume that the magnitude of the inaccuracies in the potential temperature, humidity, and wind speed of the atmospheric mixed layer are given by nonzero quantities δ_θ, δq, δ_U. These initial inaccuracies will be present because observations of the initial atmospheric state, which will be made by satellites over a large part of the ocean, will not be perfect.

Estimates for δ_θ, δq, and δ_U can be determined from the work of Moyer *et al.* (1978). They compared data deduced from the Nimbus 6 High Resolution Infrared Radiation Sounder and Scanning Microwave Spectrometer to data obtained from weighted radiosonde observations from the east central United States. They found the standard deviation between the satellite and radiosonde observations of temperature, humidity, and geostrophic wind speed at 850 mb, σ_T, σ_q, and σ_U, to be about

$$\begin{aligned} \sigma_T &= 1.5\ ^{o}C \\ \sigma_q &= 1.6\ \text{gm kg}^{-1} \\ \sigma_U &= 5\ \text{m s}^{-1} \end{aligned} \qquad (38)$$

We will take

$$\delta_\theta = \frac{1}{8}\,\sigma_T$$

$$\delta_q = \frac{1}{8}\,\sigma_q \qquad (39)$$

$$\delta_U = \frac{1}{16}\,\sigma_U$$

Thus δ_θ and δ_q are set equal to one eighth standard deviation limits. Note that because of surface friction, U_m is typically only about one half the geostrophic wind speed in the lower atmosphere. As a result, an additional factor of 1/2 arises when relating δ_U to σ_U. Therefore, the value assigned to δ_U can also be regarded as a one eighth standard deviation limit.

Moyer et al. (1978) also calculated the standard deviation between the satellite and radiosonde observations of 500 mb geopotential height, σ_Φ, and found

$$\sigma_\Phi = 15 \text{ m} \qquad (40)$$

This combined with the results of Baumhefner and Downey (1978) can be used to determine rough estimates for the rate at which the inaccuracies grow with time. Baumhefner and Downey did a forecast intercomparison study for the Northern Hemisphere using six different initial states and three different general circulation models of the atmosphere. Data from the National Meteorological Center operational analyses

were used for forecast verification. At the end of a five day forecast, the area-averaged standard deviation between the predicted and observed 500 mb geopotential height was typically 110 m. Furthermore, a good first order approximation to the results of Baumhefner and Downey is to assume that the forecast error for geopotential height increases linearly with time. Thus, taking the one eighth standard deviation limit for δ_Φ, we have

$$\Delta\Phi = \delta_\Phi (1 + \gamma t) \tag{41}$$

where $\Delta\Phi$ is the inaccuracy in 500 mb height, $\delta_\Phi = \frac{1}{8}\sigma_\Phi$, and

$$\gamma = \frac{\frac{110 \text{ m}}{15 \text{ m}} - 1}{5 \text{ days}} = 1.27 \text{ days}^{-1} \tag{42}$$

Now, temperature, humidity, wind speed, and geopotential height are expected to be well correlated with one another. Thus, it is reasonable to expect that the magnitudes of the inaccuracies resulting from imperfect forecasts of these quantities will also be well correlated with one another. Therefore, as a first approximation we take

$$\frac{\Delta\theta_m}{\delta_\theta} = \frac{\Delta q_m}{\delta_q} = \frac{\Delta U_m}{\delta_U} = \frac{\Delta\Phi}{\delta_\Phi} \tag{43}$$

which implies

$$\Delta\theta = \pm\delta_\theta (1 + \gamma t)$$
$$\Delta q = \pm\delta_q (1 + \gamma t) \qquad (44)$$
$$\Delta U = \pm\delta_U (1 + \gamma t)$$

Using (38), (39), (42), and (44), we find the functional form for $\Delta\theta_m$, Δq_m, and ΔU_m given in Table 2. Note that $\Delta\theta_m$ and Δq_m are negative and ΔU_m is positive in Experiment 9 while the reverse is the case for Experiment 10 (see Table 2). Thus, the inaccuracies in Experiment 9 all combine in such a way as to increase the flux of sensible plus latent heat from sea to air while the reverse is true for Experiment 10.

The probability that the inaccuracies in the atmospheric parameters for a real forecast situation will have the same signs as and magnitudes as least as large as those prescribed for Experiments 9 and 10 can be estimated as follows. First, we define the inaccuracies in temperature, humidity, and wind speed for a hypothetical forecast situation to be $\Delta\theta^*$, Δq^*, and ΔU^*, respectively, and assume that they are normally distributed about zero. In addition we assume that the standard deviations of these quantities at the beginning of the forecast period on some Northern Hemisphere grid are given by our earlier chosen values, δ_θ, δ_q, and δ_U. Now, if the standard deviations for $\Delta\theta^*$, Δq^*,

and ΔU^* increase at least as fast with time during the forecast period as the standard deviation of $\Delta\Phi$ based on the linear fit to the results of Baumhefner and Downey (1978), then our prescribed values for $\Delta\theta_m$, Δq_m, and U_m (see eq. 44) will always lie within the one eighth standard deviation limits for $\Delta\theta^*$, Δq^*, and ΔU^*.

Now, to obtain an estimate of the lower bound on the probability in question, we will assume for the moment that $\Delta\theta^*$, Δq^*, and U^* are completely uncorrelated with one another. From probability theory this implies that $\Delta\theta^*$, Δq^*, and ΔU^* are statistically independent which means that the joint probability distribution function for these quantities can be written as a product of the individual probability distribution functions. Therefore, based on the one eighth standard deviation limits, the probability that the magnitudes of $\Delta\theta^*$, Δq^*, and ΔU^* will be simultaneously larger than the magnitudes of our prescribed values for $\Delta\theta_m$, Δq_m, and ΔU_m is 93%. However, the probability that $\Delta\theta^*$, Δq^*, and ΔU^* will also have the same <u>signs</u> as the prescribed values in Experiment 9 is only $93\%/8 \cong 12\%$, as is also the case for Experiment 10. Thus, even if the inaccuracies in the atmospheric parameters are completely uncorrelated, we expect that they will combine to yield inaccuracies in the surface flux as least as large as those in either Experiments 9 or 10 over about 24% of the Northern Hemisphere ocean.

In reality, however, we expect that the inaccuracies in the atmospheric parameters <u>will</u> be correlated with one another. For example, $\Delta\theta^*$ and Δq^* should be very well correlated with a positive correlation coefficient as

demonstrated by the following qualitative argument. Both temperature and humidity in the lower atmosphere generally decrease from equator to pole. Therefore, if at some location during the course of the forecast period the real wind in the lower atmosphere develops a stronger poleward component than the forecast wind, horizontal advection will tend to force both $\Delta\theta^*$ and Δq^* negative. The reverse case will occur if the real wind develops a stronger equatorward component than the forecast wind, and $\Delta\theta^*$ and Δq^* will again be positively correlated. Correlation between inaccuracies in the temperature and inaccuracies in the wind speed is less obvious. This is because the inaccuracies in the wind field are related to horizontal gradients of the inaccuracies in the temperature field, rather than the temperature inaccuracies themselves.

Therefore, as a rough estimate of the upper bound on the probability that the inaccuracies will be at least as bad (from an ocean forecasting point of view) as those prescribed in either Experiments 9 or 10, we here assume that $\Delta\theta^*$ and Δq^* are perfectly correlated with each other but completely uncorrelated with ΔU^*. From arguments similar to those presented earlier in this section, we find an estimate of this upper bound to be 45%. Thus, to summarize this analysis, we expect the errors in real ocean forecasts due to inaccuracies in the air temperature, humidity, and wind speed alone to be at least as bad as either those resulting from Experiments 9 and 10 over roughly 24% to 45% of the ocean in the Northern Hemisphere.

Fig. 9 shows the results for Experiment 9. In this case, the mixed layer becomes anomalously deep and cool because of increased wind generation of turbulent kinetic

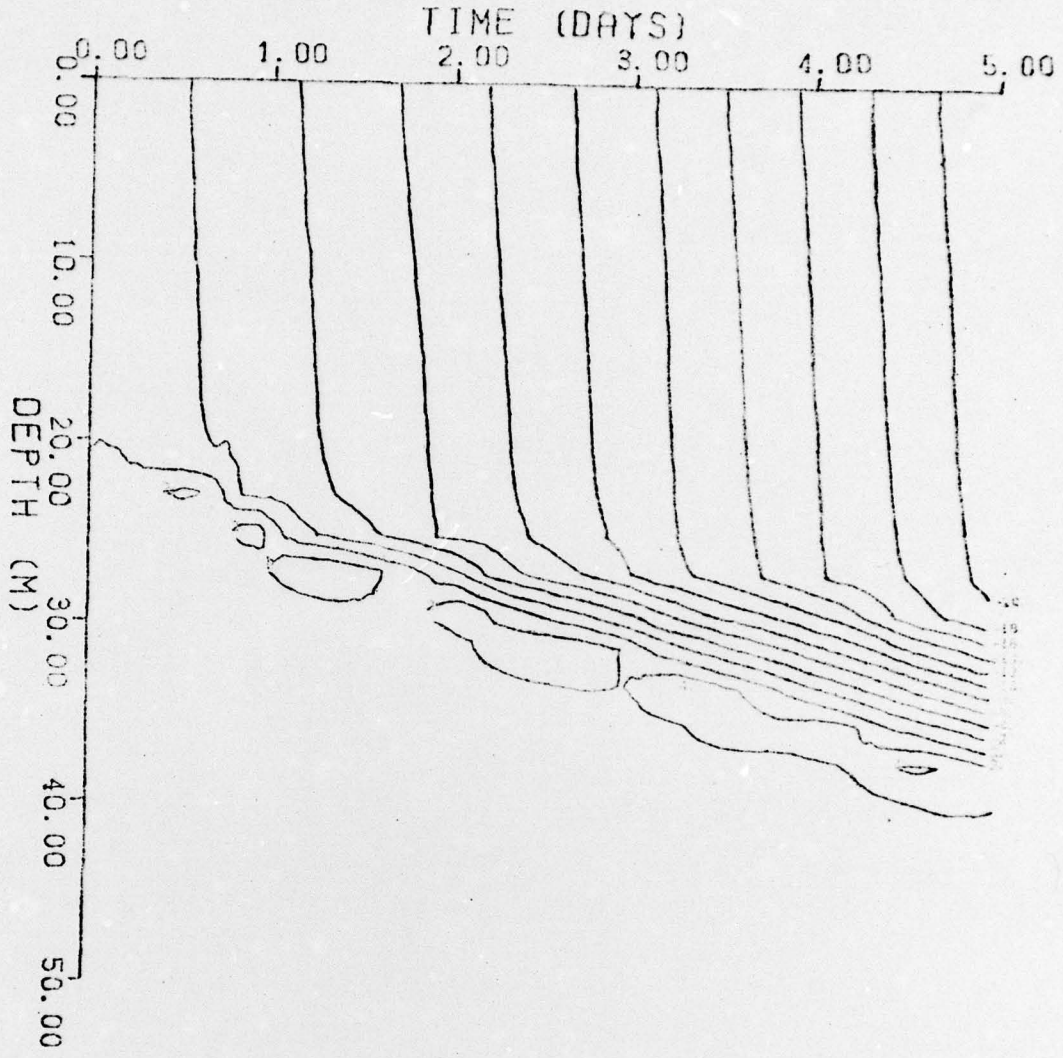

Figure 9. Same as Figure 1 but for Experiment 9 ($\Delta\theta_m = -0.187[1 + 1.27\ day^{-1}\ t]\ ^oC$, $\Delta q_m = -\ 0.2\ [1.27\ day^{-1}\ t]\ gm\ kg^{-1}$, $\Delta U_m = 0.312\ [1 + 1.27\ day^{-1}\ t]\ m\ s^{-1}$, $\Delta C = 0$).

energy in the upper ocean and increased fluxes of sensible and latent heat from sea to air. Note that the mixed layer temperature anomaly grows more rapidly near the end of the five day forecast than near the beginning. This is because the atmospheric prediction becomes progressively worse with time during the forecast period (and hence the magnitudes of $\Delta\theta_m$, Δq_m, etc. become progressively larger).

At the end of the five day period, the mixed layer is 8 m deeper than that of the Control Experiment. This accounts for the warm anomaly near the base of the mixed layer shown in Fig. 9 and represents a significant forecast inaccuracy. Also of interest on Fig. 9 is the region of large vertical gradient of temperature anomaly between 28 and 38 m depth at day five. As mentioned earlier, this concentration of the isolines of temperature anomaly near the base of the mixed layer may have important implications for acoustic prediction.

Fig. 10 shows the results for Experiment 10. The mixed layer becomes anomalously shallow and warm in this experiment because the wind generation of turbulent kinetic energy in the upper ocean and the surface fluxes of latent and sensible heat are anomalously small. As was the case for Experiment 9, the mixed layer temperature anomaly increases faster near the end of the forecast than near the beginning. Furthermore, since the average thermal inertia of the mixed layer is anomalously small in this case (because of its shallowness) the effect is even more pronounced than it was in Experiment 9.

In addition, comparison of Figs. 9 and 10 shows that the mixed layer temperature anomaly resulting at the

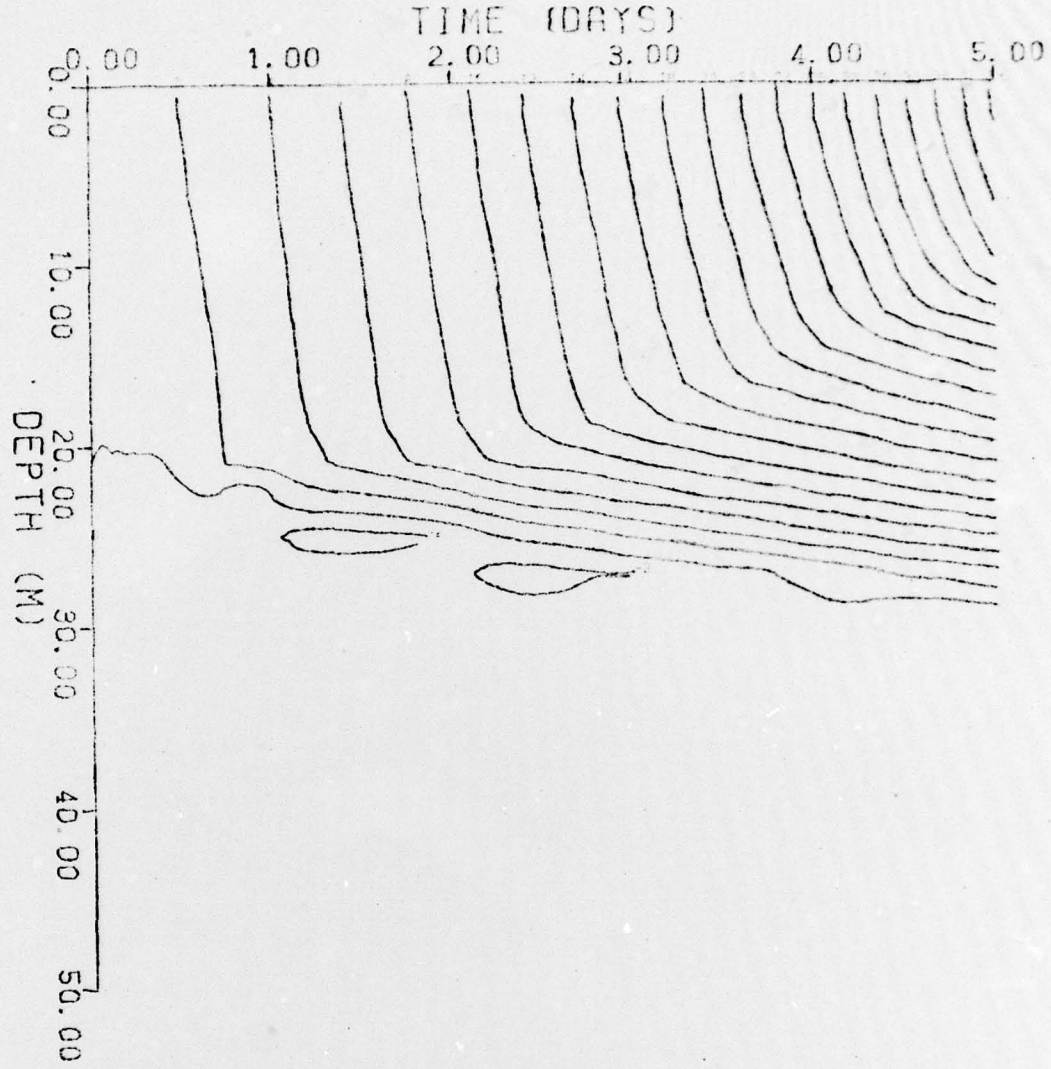

Figure 10. Same as Figure 1 but for Experiment 10 ($\Delta\theta_m = 0.187\,[1 + 1.27\ day^{-1}\ t]\ ^oC$, $\Delta q_m = 0.2\,[1 + 1.27\ day^{-1}\ t]\ gm\ kg^{-1}$, $\Delta U_m = -\ 0.312\,[1 + 1.27\ day^{-1}\ t]\ m\ s^{-1}$, $\Delta C = 0$).

end of the five day forecast is about twice as large in Experiment 10 than in Experiment 9. Since the inaccuracies in the atmospheric parameters ($\Delta\theta_m$, Δq_m, and ΔU_m) differ between Experiments 9 and 10 in sign but not in magnitude (see Table 2), this reflects the nonlinearities discussed in section 5.1.

At the end of the five day forecast, the predicted mixed layer depth for this experiment is 18 m shallower than that of the Control Experiment. This is a severe forecast inaccuracy and accounts for the region of large vertical gradient in temperature anomaly between 10 and 30 m depth.

6.0 SUMMARY AND CONCLUSIONS

We have used a one-dimensional model of the upper ocean to investigate the effect of inaccuracies in the potential temperature, specific humidity, and wind speed of the atmospheric mixed layer and the fractional cloud cover (which are all regarded as imposed meteorological parameters) on forecasts of ocean thermal structure. Vertical eddy fluxes of heat, salinity, and momentum in the oceanic mixed layer are parameterized using the Level-2 turbulence closure model of Mellor and Yamada (1974). Surface eddy fluxes of sensible heat, latent heat, and momentum are parameterized with bulk aerodynamic coefficients determined from Monin-Obukhov similarity theory. Surface fluxes of solar and infrared radiation are parameterized with the formulas of Wyrtki (1965).

A Control Experiment is performed by imposing time-invariant values for the meteorological parameters and integrating the model ocean forward in time for five days from an initial state characteristic of the summertime subtropical ocean. A set of ten additional experiments are performed by integrating the model for five days from the same initial state used for the Control Experiment but with different values for the various imposed meteorological parameters.

The predicted upper ocean thermal structure for the Control Experiment is regarded as a forecast in which the meteorological parameters are known exactly during the forecast period. The predicted thermal structures for the remaining ten experiments are considered to be those resulting when these parameters are not known exactly during this period.

Time-depth contours of temperature anomaly between each of the ten experiments and the Control Experiment, which can be thought of as the error introduced into the ocean forecast by inaccuracies in the meteorological parameters, are presented and discussed.

In all cases, the temperature anomaly diffuses rapidly downward from the surface to within a few meters of the mixed layer base. Because of the marked decrease in eddy diffusivity there, downward diffusion of the anomaly is much slower below this level. This results in a relatively large vertical gradient in temperature anomaly near the base of the mixed layer which may have important implications for acoustic modeling. Both the depth of the mixed layer and the magnitude of the mixed layer temperature anomaly are found to be nonlinear functions of the inaccuracies in the potential temperature, humidity, and wind speed. The magnitude of the anomalies in mixed layer depth and mixed layer temperature resulting from an inaccuracy in fractional cloud cover of 0.1 is small compared to the anomalies produced by inaccuracies in the temperature, humidity, and wind speed of 1^{o}, 1 gm kg^{-1}, and 1 m s^{-1}, respectively.

Estimates of the time evolution of the inaccuracies in the air temperature, humidity, and wind speed during an actual operational forecast situation are made. Expected magnitudes of the inaccuracies at the beginning of the forecast period are obtained from the satellite/radiosonde comparison study of Moyer et al. (1978). This, combined with the numerical weather prediction study of Baumhefner and Downey (1978), is used to estimate the rate at which the magnitude of the inaccuracies grow with time during the forecast period. Then, when the sign of the various inaccuracies

are chosen, rough estimates of the probability that the prescribed inaccuracies will be characteristic of an actual forecast situation are made. In both Experiments 9 and 10, for which the inaccuracies are prescribed in this manner, this probability estimate turns out to be about 12-22%.

In Experiment 9 during the entire forecast period, the signs of the inaccuracies are such that the air temperature and humidity are anomalously low and the wind speed is anomalously high. At the end of a five day forecast a mixed layer depth anomaly of 8 m and a mixed layer temperature anomaly of -0.2°C results. In Experiment 10, the inaccuracies in the three atmospheric parameters each have the same magnitude as those in Experiment 9 but opposite sign. In this case, the mixed layer depth anomaly and temperature anomaly resulting from a five day forecast are -18 m and 0.38°C respectively.

Of course these results are not general since the magnitude of the anomalies in mixed layer depth and temperature produced by the inaccuracies in the forecast atmospheric parameters depend on the initial depth of the mixed layer and the stratification below it. For example, during the winter when the mixed layer may be over 100 m deep, the magnitude of the anomalies may be only 1/3 to 1/5 of those found here. Nevertheless, the minimum prediction performance criteria for OPS requires an accuracy in temperature of 0.5°C (Grabowski and Roberts, 1978). Thus, the present study indicates that, at least when the mixed layer is shallow, errors introduced by inaccuracies in the meteorological forcing alone can amount to a substantial part of the minimum prediction performance criterion.

Errors introduced into ocean forecasts due to inaccuracies in the atmospheric forcing will be largest in the mixed layer. Fortunately, because of satellite observations of sea surface temperature, the initial inaccuracies in mixed layer temperature for an ocean forecast will be relatively small. Thus, a trade off situation exists. Inaccuracies in the atmospheric forcing will introduce errors into forecasts of the upper ocean, but the initial conditions for the forecast will be relatively good there. Inaccuracies in the atmospheric forcing will have little effect on the forecast state of the deep ocean, but the initial conditions for the forecast will be relatively bad there.

The present study can be extended in several ways. Numerical weather prediction studies using data routinely generated by an operational forecast model and analysis program could be done with particular regard for the fields that are important to the ocean forecast problem. In addition, spatial and seasonal variability of the atmospheric forecast errors might be obtained. For example, the errors may be generally small in the trade wind region compared to those of the midlatitudes, where they may be especially large in winter.

Upwelling and downwelling are induced in the mid ocean by surface wind stress curl. Thus, forecast errors of wind stress curl should also be analyzed. If these errors prove to be large enough, then a study similar to the present one should be performed with a three-dimensional model.

APPENDIX

LIST OF SYMBOLS

a	thermal expansion coefficient for seawater
A_H, A_M	stability functions for eddy coefficients in oceanic mixed layer
b	saline expansion coefficient for seawater
$b*$	Stefan-Boltzmann constant
B_o	surface flux of infrared radiation
c, c_p	specific heat at constant pressure for seawater, air
C	fractional cloud coverage
C_θ, C_q, C_m	drag coefficient for sensible heat, latent heat, momentum
E	turbulent kinetic energy
f	Coriolis parameter
F	downward flux of solar radiation
F_o, F_i	downward flux of solar radiation at sea surface, daily-averaged downward flux of solar radiation at sea surface for cloudless conditions
g	acceleration of gravity
H_o	surface flux of sensible heat
K_H, K_S, K_M	eddy diffusion coefficients for heat, salinity, and momentum
L	Monin-Obukhov stability length
L_v	latent heat of evaporation for water
l	turbulence length scale
n_1-n_8	empirical constants in eddy diffusion model
P_o	precipitation rate at sea surface
q, q_m	water vapor mixing ratio, water vapor mixing ratio of the atmospheric mixed layer
q_o, q_r, q_{10}	water vapor mixing ratio at sea surface, reference height, ten meters height
Q_o	surface evaporation rate

R_f	flux Richardson number
S	salinity
S_w, S_o	reference salinity, salinity at sea surface
T	temperature
T_w, T_o, T_{10}	reference temperature, temperature at sea surface, temperature at ten meters height
t	time
U_m	wind speed of atmospheric mixed layer
U_o, U_r	wind speed at sea surface, wind speed at reference height
u_*	surface friction velocity in air
$\underset{\rightarrow}{V}_r$	wind velocity vector at reference height
$\underset{\rightarrow}{V}_m$	wind velocity vector of the atmospheric mixed layer
$\underset{\rightarrow}{v}$, $\underset{\rightarrow}{v}_o$	current velocity vector, current velocity vector at sea surface
x,y,z	Cartessian coordinates, x positive eastward, y positive northward, z positive upward from the sea surface
$\hat{i}, \hat{j}, \hat{k}$	unit vectors in the x,y,z directions
z_r, z_o	reference height, surface roughness length
ε	infrared emissivity of sea surface
$\delta_\theta, \delta_q, \delta_u, \delta_\phi$	initial inaccuracies of potential temperature, water vapor mixing ratio, wind speed, geopotential height
κ	von Karman's constant
$\sigma_T, \sigma_q, \sigma_u, \sigma_\phi$	standard deviation of inaccuracies in temperature, water vapor mixing ratio, wind speed, geopotential height
ρ	density
ρ_w, ρ_a	reference density for water, air
θ, θ_m	potential temperature, potential temperature of atmospheric mixed layer
θ_o, θ_r	potential temperature at sea surface, potential temperature at reference height

Φ	geopotential height of 500 mb surface
ϕ_θ, ϕ_q, ϕ_m	nondimensional vertical derivatives of temperature, water vapor mixing ratio, and wind speed in the atmospheric surface layer
$\underset{\rightarrow}{\tau}_o$	surface wind stress vector
$\Delta\theta_m$, Δq_m, ΔU_m, ΔC	prescribed inaccuracies in θ_m, q_m, U_m, and C
$\Delta\theta_m^*$, Δq_m^*, ΔU_m^*	inaccuracies in θ_m, q_m, and U_m for a hypothetical forecast
$\Delta\Phi$	inaccuracy in Φ
$(^-)$	spatial average at constant z taken across a region large enough to encompass a statistically significant sampling of all unresolved phenomena
$(')$	departure from above defined spatial average
X	vector cross product

REFERENCES

Baumhefner, D. and P. Downey, 1978. Forecast intercomparisons from three numerical weather prediction models. Mon. Wea. Rev., 106, 1245-1279.

Busch, N. E., 1977. Fluxes in the surface boundary layer over the sea. Chapter 6, Modelling and Prediction of the Upper Layers of the Ocean, Pergamon Press, New York.

Businger, J. A., 1975. Interactions of sea and atmosphere. Rev. Geophys. and Space Phys., 13, 720-726.

Clarke, R. H., 1970. Recommended methods for the treatment of the boundary layer in numerical prediction models. Mon. Wea. Rev., 97, 77-85.

Grabowski, W. J., and G. O. Roberts, 1978. A sigma coordinate ocean forecasting computer code. I. Model differential equations, spatial finite-difference representation and conservation properties. Tech. Report SAI-78-721-WA. Science Applications, Inc., 8400 Westpark Drive, McLean, Virginia.

Grassl, H., 1976. The dependence of the measured cool skin of the ocean on wind stress and total heat flux. Bound. Lay. Met., 10, 465-474.

Hogstrom, U., 1974. A field study of the turbulent fluxes of heat, water vapor and momentum at a "typical" agricultural site. Quart. J. Roy. Met. Soc., 100, 624-639.

Jacobs, C. A., 1978. Numerical simulations of the natural variability in water temperature during BOMEX using alternative forms of the vertical eddy exchange coefficients. J. Phy. Ocean., 8, 119-141.

Jerlov, N. G., 1951. Optical studies of ocean waters. Rept. of the Swedish Deep Sea Exp., Vol. 3, No. 1, p. 3-59 (Goteborg).

Kolmogoroff, A. N., 1942. The equations of turbulent motion in an incompressible fluid. Izv. Akad. Nauk SSR, Ser. Fig., 6, No. 1, 2, 56-58.

Mamayev, O. I., 1958. The influence of stratification on the vertical turbulent mixing in the sea. Bull. Acad. Sci. USSR Geophys. Ser., 7, 494-497.

Martin, P. J., 1976. A comparison of three diffusion models of the upper mixed layer of the ocean. NRL Memorandum Report 3399, Naval Research Laboratory, Washington, D. C.

Mellor, G. L., and T. Yamada, 1974. A hierarchy of turbulence closure models for planetary boundary layers. J. Atmos. Sci., 31, 1791-1806.

_____, and P. A. Durbin, 1975. The structure and dynamics of the ocean surface mixed layer. J. Phy. Ocean., 5, 718-728.

Monin, A. S. and A. M. Obukhov, 1954. Basic laws of turbulent mixing in the ground layer of the atmosphere, Akad. Nauk. SSSR, Geofiz. Inst. Trudy, 151, 163-187.

Moyer, V., J. R. Scoggins, N-M. Chou, and G. S. Wilson, 1978. Atmospheric structure deduced from routine Nimbus 6 satellite data. Mon. Wea. Rev., 106, 1340-1352.

Munk, W. and E. R. Anderson, 1948. Notes on a theory of the thermocline. J. Mar. Res., 7, 276-295.

Pandolfo, J. P., 1969. Motions with inertial and diurnal period in a numerical model of the navifacial boundary layer. J. Mar. Res., 27, 301-317.

Rotta, J. C., 1951. Statistiche theorie michthomogener turbulenz. Z. Phys., 129, 547-572.

Vager, B. G., and S. S. Zilitinkevich, 1968. A theoretical model of the diurnal variations of the meteorological fields. Meteorol. i. Gidrol, 7.

Wyrtki, K., 1965. The average annual heat balance of the North Pacific Ocean and its relation to ocean circulation. J. Geophys. Res., 70, 4547-4559.